DOI 10.1007/s10946-023-10174-2
Journal of Russian Laser Research, Volume 44, Number 6, November, 2023

AN APERTURELESS SCANNING NEAR-FIELD OPTICAL MICROSCOPE PROBE WITH A LATERAL RESOLUTION OF 10 – 15 nm OBSERVED WITH A SEMICONDUCTOR STRUCTURE

D. V. Kazantsev,[1,2,3*] A. V. Klekovkin,[1] I. I. Minaev,[1] E. A. Kazantseva,[4] and S. N. Nikolaev[1]

[1] *Lebedev Physical Institute, Russian Academy of Sciences*
Leninskii Prospect 53, Moscow 119991, Russia

[2] *NT-MDT Spectrum Instrument*
Lane 4922, 4, Bldg. 3, Zelenograd 124482, Moscow, Russia

[3] *Higher School of Economy (HSE)*
St. Basmannaya str. 21/4, Moscow 105066, Russia

[4] *MIREA Russian Technological University*
Vernadskogo Prospect 78, Moscow 119454, Russia

[*]Corresponding author e-mail: kaza@itep.ru

Abstract

Using InSb/GaSb semiconductor quantum dots, we demonstrate the lateral spatial resolution of scattering apertureless near-field microscope equal to 10 – 15 nm at a wavelength of $\lambda = 10.7$ μm provided by a single-mode CO_2 laser. The measurement conditions make it possible to undoubtedly exclude any artifacts caused by the sample topography and other similar factors. We identify the strongly localized in-plane near-field signal with a two-dimensional electron gas clamped on the InSb/GaSb interface of quantum dots.

Keywords: Scanning near-field optical microscopy (SNOM), scanning probe microscopy (SPM), apertureless SNOM (ASNOM), nanostructure, ASNOM of elastic light scattering (sSNOM).

1. Introduction

In the mid-1980s, a wide group of instruments appeared in the everyday life of experimental techniques united by the name of scanning probe microscopy (SPM). A significant place among them belongs to scanning near-field optical microscopy (SNOM). In such a kind of instruments, the interaction between an instrument and an object under study occurs in the local light fields, concentrated in the vicinity of a probing tip apex.

Imaging lateral resolution of SNOM was introduced in the first publications [1, 2] as a modest value of $\lambda/10$, just ten-fold better than a wavelength. After the skepticism generated by the uncertainty relations [3, 4] passed, scientists realized that such a limitation concerns only the waves. As for the electromagnetic field itself, it can be applied with a wire to the object under study with any, even atomic, spatial resolution. Optical imaging lateral resolution of the first (aperture-defined) SNOMs was reported

Manuscript submitted by the authors in English on September 28, 2023.

as 50 nm (Al letters on a glass, $\lambda = 514$ nm [5]), as 60 nm (carbocyanin in polymethyl methacrylate (PMMA) luminescence, $\lambda = 650$ nm [6]), and as 90 nm (Rhodamin-6G luminescence, $\lambda = 650$ nm [7]). Nevertheless, all aperture-defined SNOMs have a common disadvantage – light transmission through tiny pinhole drops down [8, 9] much faster than the hole geometric area πa^2. In fact, light transmission through a tapered fiber was measured [10, 11] as $10^{-5} - 10^{-6}$ of injected light power.

Soon after that, an apertureless SNOM (ASNOM) was invented [12–14]. ASNOM is a more predictable and sensitive technique based on a light interaction of a sample with electromagnetic fields concentrated around the tip apex. As a rule, a pyramidal-shaped tip is covered with a metal layer (usually, Pt) to improve its optical response.

The operation of an sSNOM (ASNOM of elastic light scattering, without any frequency shift) is, in common acceptance, as described below (Fig. 1). An external laser beam irradiates an elongated probing tip (it looks similar to a rod dipole antenna in classical radiophysics). Local electromagnetic field $E(\omega)$ at a light frequency ω around a tip excites driven dipole oscillations in it, which can be described with a tip polarizability $\alpha_{\text{tip}}(\omega)$. These dipole oscillations, in turn, emit a divergent light wave into a surrounding space. Tip-sample distance is modulated in an sSNOM due to TappingMode$^{\text{TM}}$ operation of a topography feedback, with a mechanical frequency $f_{\text{tip}} = 30 - 300$ kHz and amplitude $z_0 = 20 - 200$ nm. Most part of oscillation period such an "antenna rod" (oriented normal to the surface) is electrodynamically free, because tip-sample separation distance is large. At the moment of a tip-sample bounce, this optical antenna gets "grounded" at its end via nano-capacitor between tip apex and sample. The lateral dimension of such a nano-capacitor determines a spatial resolution of an ASNOM at optical wavelength and corresponds to the tip apex radius. Effective polarizability $\alpha_{\text{tip}}(\omega)$ of a tip (considered together with its electromagnetic "image" in a sample surface under study) gets changed at the moment of "contact." It causes a sharp change in the amplitude and phase of a light wave scattered by a tip. Such a change can be optically detected in a far zone, e.g. with an optical homo-(hetero)-dyning in an interferometer. Assuming driving field $E(\omega)$ to be constant all the time, the amplitude A and phase φ of a recovered sSNOM signal depend mainly on a sample dielectric function $\varepsilon_s(x, y)$ at each surface point (x, y), with its real ε_s' and imaginary ε_s'' parts. If a sample surface consists of different materials with their different dielectric function $\varepsilon_s(x, y)$, sSNOM 2D-scanning of a surface provides a material contrast on a map.

Lateral resolution of ASNOM were reported as 0.8 nm [15], 1 nm [16], 10 nm [17], 30 nm [18], and 50 nm [19]. However, the optical near-field interaction is a short-range one not only in the sample plane. It is enough to retract a tip of 20 – 30 nm from the sample surface to drop down the near-field component of the tip–sample optical interaction completely. Due to that, the observed change in a collected ASNOM signal over a tiny "dust piece" can be just an artifact, with no true relation to sample's local optical properties. Due to that, changes in optical signal with a characteristic scale of 1 nm [14] in a sample plane are not completely convincing. Optical images of the oil droplets on a mica surface [16] demonstrate no doubtless correlation between optical and topographical maps – some optical images of the droplets are wider, and some images are narrow compared to their topographical images. A lateral resolution of 1 nm is claimed by the best droplet image.

Semiconductor samples of modulated doping profile [20, 21] are also not perfect objects to calibrate doubtless lateral resolution of ASNOM. It is stated by vendors that the doping profile of the silicon structure impurities forms a step sharper than 10 nm. Despite that, the sSNOM amplitude and phase signal (depending on free-carrier plasma concentration in a semiconductor) collected over a sample cleavage across the doping layers is often blurred to a characteristic scale of 70 – 100 nm in the sample surface

plane. Thus, sharp surface structures, such as quantum dots (QD), can be a good test object for investigating the possibilities of ASNOM. In addition, QDs are used in a number of practical applications, for example, laser sources [22].

2. Samples and Setup

InSb QDs are grown by a Compact-21t (RIBER) MBE setup. For epitaxial growth, epi-ready GaSb (100) substrates are used. In the Stransky–Krastanov process, the material to be grown first forms a continuous layer on the surface of the substrate until its thickness reaches a critical value of 1.5 ML. After that, 3D growth begins, in which QDs themselves get formed. Growth rates of In and Ga are calibrated by the oscillations in RHEED (Reflection High Energy Electron Diffraction) data. To remove oxides from a substrate surface, temperature $530 \pm 10°$C is used. After that, a GaSb buffer layer of ∼250 nm thickness is grown at the temperature equal to $500 \pm 10°$ C. InSb QDs are grown at the temperature equal to 300°C. Growth rate of In and Sb are determined by the pressure of $\sim 1.3 \cdot 10^{-7}$ Torr for In and from $5 \cdot 10^{-6}$ to $8 \cdot 10^{-7}$ Torr for Sb. The growth time for InSb QDs is 60 – 80 s, with a growth rate of 0.13 ML/s.

To carry out an ASNOM surface mapping in elastic scattering mode (SSNOM), we use a traditional SSNOM setup [23]; see Fig. 1. A coherent laser beam is focused onto a probing tip and drives the dipole oscillations in it. Electromagnetic waves scattered by a tip are collected back into a Michelson interferometer and reach a photodetector together with a reference beam. NT-MDT Spectrum Instruments (Russia) offers equipment for such operational mode. We use SPM controller Nova to manage TappingMode surface scanning and to store sSNOM signal as a 2D data, together with the topography and other SPM data. Probing tips FMG01/Pt with cantilever resonant frequency $f_{\text{tip}} = 60 - 80$ kHz are used. In our experiments, we use a tip oscillation amplitude z_0 of approximately 50 – 70 nm. This time, we calibrate the sensitivity of a quad photodiode tip displacement sensor by an approach curve. Such a

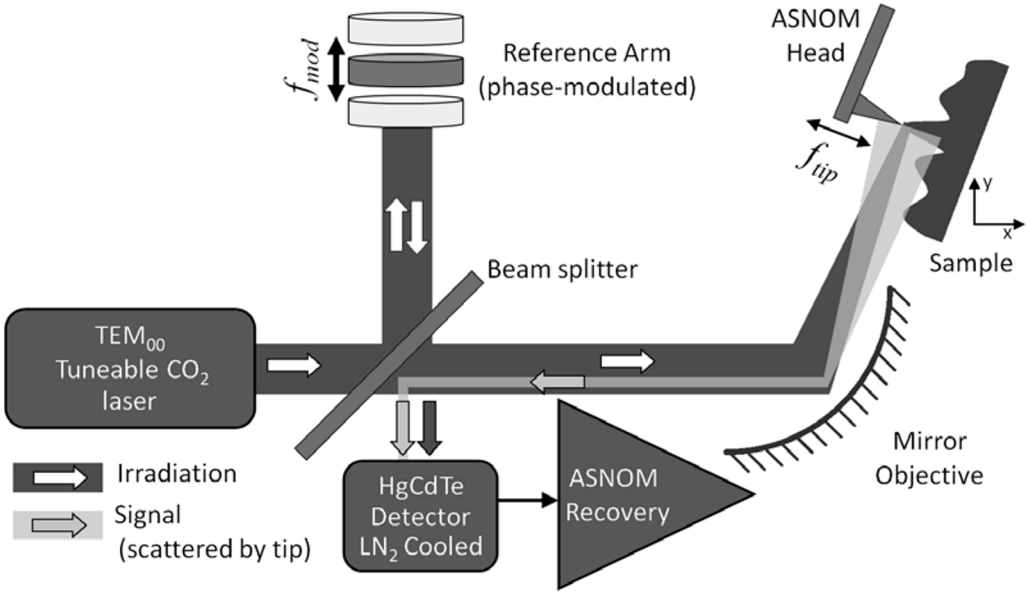

Fig. 1. The scheme of the sSNOM setup.

way provides us with a sensitivity value rather close compared to a completely decent calibration of a tip displacement with a grating of known groove height [24]. As a source of coherent light, we use a tunable CO_2 laser Merit-G (Laser Access, USA).

The radiation with $\lambda \approx 10.7$ μm at the output of the Michelson scheme is finally received by a LN_2-cooled MCT photodetector (Teledyne Judson Technologies, USA), with a response time of 1 μs. The photodetector is connected to an input of hand-made low-noise preamplifier [25], with a bandwidth of about 1 MHz. Such the bandwidth seems to be sufficient for a transfer phase fidelity of the higher harmonic component of the tip–sample distance variation frequency f_{tip}, which, in our case, does not exceed 100 kHz.

To specifically recover the near-field component in a photocurrent signal, we use analog input–output acquisition card P25M (Innovative Integration, USA). This card is equipped with four 16 bit ADC and four 16 bit DAC channels, with a maximum rate of 25 MSPS each. Digital data can be pre-processed in FPGA and DSP of a card and then sent to a host computer via PCI slot. Input ADC measures the photocurrent signal with a $(16 \dots 64) \cdot f_{\text{tip}}$ sampling rate, then our hand-made software [26] recovers one of the higher harmonic components $f_{\text{tip}}^{(n)}$ within each tip oscillation period, yielding a complex number as result. This value depends, by a sinusoidal law, on a reference beam optical phase in the Michelson setup. Simultaneously, the acquisition card regularly ($f_{\text{mod}} = 100$ Hz) modulates the phase of a reference beam, driving a mirror by a saw-tooth law. To do that, one of the DAC channels is connected to the input of S316 piezo-stage control electronics (Physik Instrumente, GmbH, Germany). After averaging over 360° turn of the optical phases in a reference beam, a complex number is calculated, corresponding to the near-field signal phase and amplitude. These two components are electrically transferred from P25M card DAC outputs to the inputs of the main controller of SPM. As a result, the SPM controller is able to save the acquired 2D map of an sSNOM signal to the HDD, together with collected maps of topography, cantilever oscillation, amplitude/phase, etc.

3. Results and Discussion

An image of self-assembled QDs array grown on a GaSb substrate is presented in Fig. 2. Here, the topography image is presented in part (T), and a map of the tip vibration phase, measured in Tapping Mode™ in order to keep optimum "touch grade" between the probing tip and the sample surface is presented in part (V). The bottom parts of Fig. 2 contain the sSNOM signal amplitude (A) and phase (φ), respectively, recovered in a detector signal at the output of a Michelson interferometer setup. We acquire the second harmonic $f_{\text{tip}}^{(2)}$ component of a tip oscillation frequency, followed by its averaging over all phases of the homodyning beam light.

One should point out, that ASNOM phase signal shown in part (φ) of Fig. 2 is determined not by ideal but by real mode of the tip oscillation in respect to a sample surface. In particular, deviation of the V signal (phase of a tip mechanical oscillation) causes a shift of φ component obtained in a photocurrent. For the purpose of revealing the artifacts of the optical phase measurement in the sSNOM signal, these two signals are placed in Fig. 2 next to each other. Comparing these two images, one can find that both phase deviation signals are small. The few clearly dark spots in both images are caused by "palette puncture" – when the detected phase exceeds a maximum value of +180° (depicted in the palette as the brightest color), it acquires a value of −180°, which is the darkest color on the palette.

The undoubted correlation of parts (V) and (φ) in Fig. 2 allows us to state that there are no noticeable

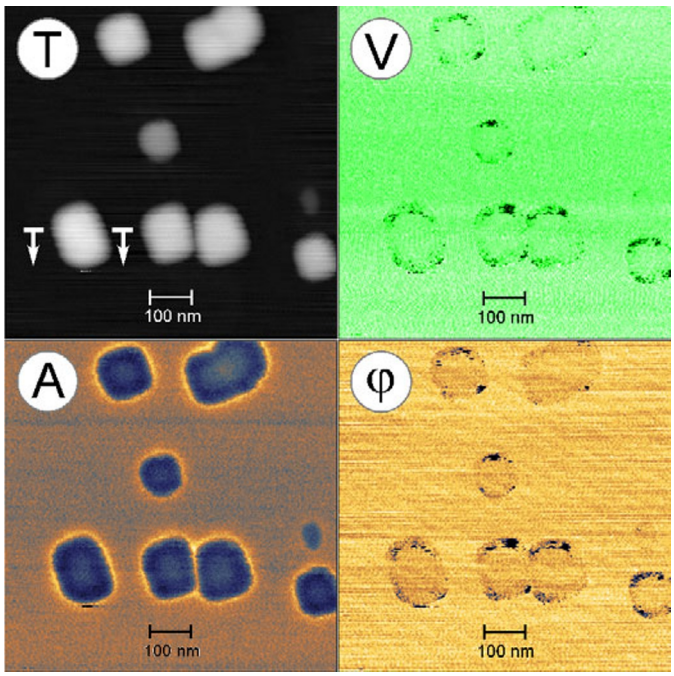

Fig. 2. ASNOM image of self-assembled InSb QDs array grown on a GaSb substrate. Here, the topography image (T), the phase of a cantilever vibration in a Tapping Mode™ (V), amplitude (A) and phase (φ) of the second harmonic component $f_{\text{tip}}^{(2)}$ in a photocurrent at the Michelson interferometer setup output. The tunable CO_2 laser at wavelength $\lambda = 10.7$ μm ($\nu = 935$ cm^{-1}) is used in the experiment.

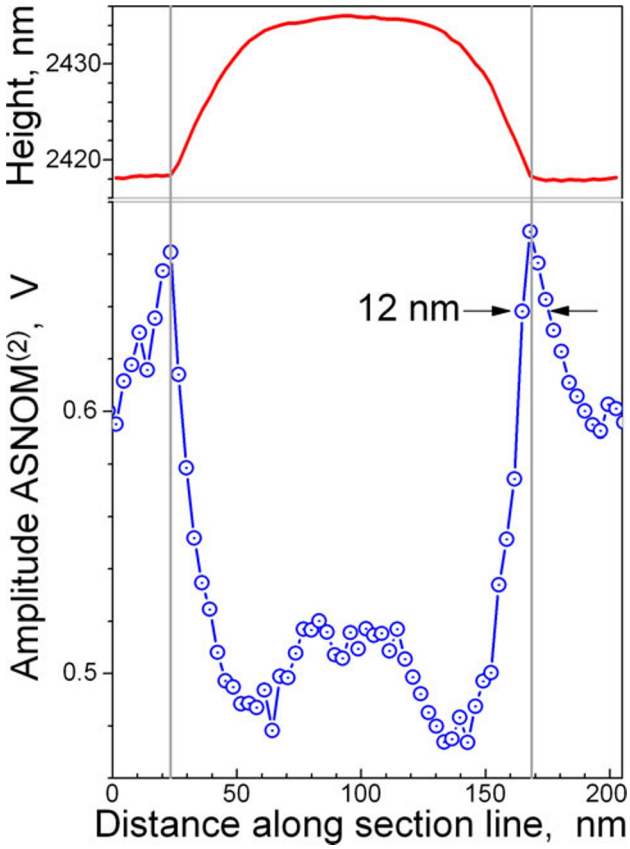

Fig. 3. Cross-sectional profiles of topography image (T) and ASNOM-amplitude (A) along the line indicated in Fig. 2 (T).

variations in the phase of the ASNOM signal in the experiment.

This is not at all the case with the recorded amplitude of the ASNOM signal (A). ASNOM image around each quantum dot contains a clearly distinguishable halo of increased signal amplitude. In Fig. 3, we show a section of the signal map topographic height (T) and amplitude of the optical near-field signal (A). The position of the beginning and end of the section line is shown by marks in part (T) of Fig. 2.

Change of detected ASNOM-signal amplitude in our experiment takes place at 10 – 15 nm length along the sample surface. The characteristic scale of "lateral resolution" depends on the tip instance and on its wear. We can point out the absence of any features in the topography image in all cases of "halo" observation in the ASNOM signal. This makes it possible to completely exclude the hypothesis of a drop in the recorded ASNOM amplitude caused by the retracting of the probing tip from the sample during surface scanning. As one can see in Fig. 3, the surface of the sample is almost smooth. A typical QD height is 15 – 20 nm with a total image width of 800 nm and a single quantum dot width of 150 nm, i.e., with physical proportions height–width of 2.5% and 10%, respectively.

Due to the energy band tailoring on the interface QD/substrate [27], the quantum dot is expected to be charged. Acting as a static Coulomb charge, the QD can attract some free electrons from GaSb

substrate.

In a sample scanning process, as the probing tip moves away from a QD (here, its optical response is determined mainly by InSb layer, with a thickness of 15 nm, onto substrate surface), the tip grounding conditions change sharply. Instead of the QD response (its dielectric function is mainly real), the tip probes now the GaSb substrate through a very thin wetting layer. Dielectric response of the substrate, in addition to its real part ε_s', contains also a noticeable imaginary component ε_s'', caused by the presence of free carriers in the bulk substrate. Thus, outside the QD dielectric disk, we observe a sharp step of the sSNOM signal near its edge, just due to material contrast usually provided by an sSNOM, corresponding to the local value of $\varepsilon_s(x, y)$ on a sample surface. For a similar reason, a 10 nm thick Si_3N_4 layer embedded in Si is clearly imaged in a cleaved transistor structure [20].

Far of electrostatic charges located in QD, the carrier plasma concentration in a substrate surface decreases smoothly, with a characteristic length L_{xy} of ≈ 40 nm, and the sSNOM signal gets to its average value over the GaSb surface also.

4. Summary

We observed ASNOM images of InSb/GaSb semiconductor quantum dots with a feature width of 10–15 nm. In our case, it can be clearly interpreted as a lateral imaging resolution of probing tips FMG01/Pt being used. We observed the absence of any features in a topography image at the points of significant changes in the optical signal, and also a stability of the phase of the probe mechanical oscillation during scanning. These observations allow us to confidently reject the hypothesis of instability in the degree of tip–sample contact as a reason for optical signal changes.

Acknowledgments

This study was supported by the Russian Science Foundation under Grant No. 19-79-30086.

References

1. D. W. Pohl, W. Denk, and M. Lanz, *Applied Physics Letters*, **44**, 651 (1984); DOI: 10.1063/1.94865
2. U. Dürig, D. W. Pohl, and F. Rohner, *Journal of Applied Physics*, **59**, 3318 (1986); DOI: 10.1063/1.336848
3. E. Abbe, *Archiv für Mikroskopische Anatomie*, **9**, 413 (1873); DOI: 10.1007/BF02956173
4. W. Heisenberg, *Zeitschrift für Physik*, **43**, 172 (1927); DOI: 10.1007/BF01397280
5. E. Betzig, J. K. Trautman, T. D. Harris, et al., *Science*, **251**, 1468 (1991); DOI: 10.1126/science.251.5000.146
6. E. Betzig and R. J. Chichester, *Science*, **262**, 1422 (1993); DOI: 10.1126/science.262.5138.1422
7. W. P. Ambrose, P. M. Goodwin, J. C. Martin, and R. A. Keller, *Phys. Rev. Lett.*, **72**, 160 (1994); DOI: 10.1103/PhysRevLett.72.160
8. H. A. Bethe, *Phys. Rev.*, **66**, 163 (1944); DOI: 10.1103/PhysRev.66.163
9. C. Bouwkamp, *Philips Res. Rep.*, **5**, 401 (1950).
10. G. A. Valaskovic, M. Holton, and G. H. Morrison, *Appl. Opt.*, **34**, 1215 (1995); DOI: 10.1364/AO.34.001215
11. A. A. Kolesnikov, Y. E. Lozovik, and S. P. Merkulova, *J. Russ. Laser Res.*, **31**, 469 (2010); DOI: 10.1007/s10946-010-9168-9
12. H. Wickramasinghe and C. Williams, "Apertureless near field optical microscope," Patent, Aug. 7, 1990, US Patent 4,947,034; `www.google.com/patents/US4947034`
13. Y. Inouye and S. Kawata, *Opt. Lett.*, **19**, 159 (1994); DOI: 10.1364/OL.19.000159

14. F. Zenhausern, M. P. O'Boyle, and H. K. Wickramasinghe, *Appl. Phys. Lett.*, **65**, 1623 (1994); DOI: 10.1063/1.112931
15. Y. Martin, F. Zenhausern, and H. K. Wickramasinghe, *Appl. Phys. Lett.*, **68**, 2475 (1996); DOI: 10.1063/1.115825
16. F. Zenhausern, Y. Martin, and H. K. Wickramasinghe, *Science*, **269**, 1083 (1995); DOI: 10.1126/science.269.5227.1083
17. A. Bek, R. Vogelgesang, and K. Kern, *Rev. Sci. Instr.*, **77**, 043703 (2006); DOI: 10.1063/1.2190211
18. M. Brehm, T. Taubner, R. Hillenbrand, and F. Keilmann, *Nano Lett.*, **6**, 1307 (2006); DOI: 10.1021/nl0610836
19. P. M. Bridger and T. C. McGill, *Opt. Lett.*, **24**, 1005 (1999); DOI: 10.1364/OL.24.001005
20. A. J. Huber, D. Kazantsev, F. Keilmann, et al., *Adv. Mater.*, **19**, 2209 (2007); DOI: 10.1002/adma.200602303
21. D. V. Kazantsev, E. A. Kazantseva, E. V. Kuznetsov, et al., *Bull. Russ. Acad. Sci. Phys.*, **81**, 1511 (2017); DOI: 10.3103/S1062873817120176
22. N. Gupta, A. Yelashetty, A. Sharma, et al., *J. Russ. Laser Res.*, **41**, 86 (2020); DOI: 10.1007/s10946-020-09851-3
23. F. Keilmann and R. Hillenbrand, *Philos. Trans. Royal Soc. A*, **362**, 787 (2004); `www.jstor.org/stable/4142390`
24. D. V. Kazantsev and E. A. Kazantzeva, *Instrum. Exp. Tech.*, **57**, 631 (2014); DOI: 10.1134/S0020441214040046
25. D. V. Kazantsev and E. A. Kazantseva, *Instrum. Exp. Tech.*, **63**, 133 (2020); DOI: 10.1134/S0020441220010194
26. D. V. Kazantsev and E. A. Kazantseva, *Instrum. Exp. Tech.*, **65**, 273 (2022); DOI: 10.1134/S0020441222020130
27. S. I. Rybchenko, G. Yeap, R. Gupta, et al., *J. Appl. Phys.*, **102**, 013706 (2007); DOI: 10.1063/1.2752127